

Steady state sedimentation of ultrasoft colloids

Sunil P. Singh

*Indian Institute of Science Education and Research Bhopal,
Bhopal by pass road Bhauri, Bhopal 462 066, Madhya Pradesh, INDIA**

Gerhard Gompper and Roland G. Winkler

*Theoretical Soft Mater and Biophysics, Institute for Advanced Simulation and Institute of Complex Systems,
Forschungszentrum Jülich, D-52425 Jülich, Germany[†]*

(Dated: May 3, 2022)

The structural and dynamical properties of ultra-soft colloids—star polymers—exposed to a uniform external force field are analyzed applying the multiparticle collision dynamics approach, a hybrid coarse-grain mesoscale simulation approach, which captures thermal fluctuations and long-range hydrodynamic interactions. In the weak field limit, the structure of the star polymer is nearly unchanged, however in an intermediate regime, the radius of gyration decreases, in particular transverse to the sedimentation direction. In the limit of a strong field, the radius of gyration increases with field strength. Correspondingly, the sedimentation coefficient increases with increasing field strength, passes through a maximum and decreases again at high field strengths. The maximum value depends on the functionality of the star polymer. High field strengths lead to symmetry breaking with trailing, strongly stretched polymer arms and a compact star polymer body. In the weak field linear response regime, the sedimentation coefficient follows the scaling relation of a star polymer in terms of functionality and arm length.

I. INTRODUCTION

External fields are able to induce drastic conformational changes of soft materials, such as polymers, colloids, vesicles etc. In turn, their dynamical and transport properties are modified, an effect which can be exploited in technical applications [1, 2]. The understanding of the relation between the nonequilibrium structure and the transport coefficients is fundamental for the rational design of novel functional materials as well as the understanding of the functional principles of biological systems. The intriguing nonequilibrium properties of soft matter in shear and Poiseuille flow have been illustrated for linear [3–13] and star polymers [14–18] as well as vesicles [19–27] and blood cells [28–37].

In nature, large macromolecular or colloidal particles sediment to the bottom of a container due to the gravitational force and the density difference of the particles and the solvent. Technically, gravity-driven motion is exploited in analytical ultra-centrifuge techniques for the characterization and separation of synthetic and biological molecules from mixtures [38, 39]. Sedimentation of colloidal and polymeric systems is enormously important for scientific and engineering applications, because soft materials whose size and shape are sensitive to thermal fluctuations and weak external flows, exhibit interesting, and *a priori* unexpected physical behavior. An example is the sedimentation coefficient of DNA molecules in a dilute suspension, which decreases with the increas-

ing driving force [40], denoted as sedimentation anomaly. It is explained by inhomogeneous hydrodynamic interactions of the polymer coil [41–43]. The coil exterior, especially the chain ends, experience a higher drag, while the monomers in the interior are hydrodynamically shielded. This implies a deformation of the coil and a decreasing sedimentation coefficient [41, 44]. Indeed, the computer simulations of Refs. [41, 44] reveal intriguing conformational changes of the polymer coil with a strong polymer stretching of the trailing end and the formation of a rather compact polymer coil.

In the present work, we investigate the steady-state sedimentation properties of dilute suspensions of the ultrasoft colloids—star polymers. These colloids are particularly interesting due to their intrinsic nature to inhibit colloidal and polymeric properties [15, 17, 18, 45]. A star polymer is a special type of branched polymer, comprised of several flexible linear polymers which are attached to a common center. The number of polymer arms controls the properties of the colloid—a small number of arms leads to polymer-like behavior and a large number of arms to colloidal behavior. The equilibrium and nonequilibrium properties of star polymers have been addressed in various experimental and simulation studies [14–18, 46–53].

Hydrodynamic interactions are essential for the sedimentation of polymers, as discussed, e.g., in Ref. [41]. To adequately account for fluid-mediated interactions, we combine molecular dynamics (MD) simulations of a star polymer with the multiparticle collision dynamics (MPC) approach for the fluid [54–56]. MPC is a particle based simulation approach, which provides a solution of the Navier-Stokes equations on appropriate length and time scales [57–59]. It includes thermal fluctuations and is excellently suited for a combination with MD simula-

*Electronic address: spsingh@iiserb.ac.in

[†]Electronic address: g.gompper@fz-juelich.de; r.winkler@fz-juelich.de

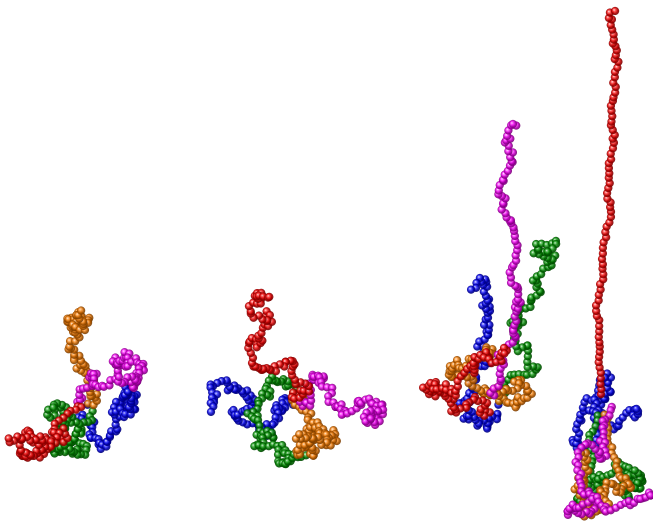


FIG. 1: Snapshots of a sedimenting star polymer for the arm number $f = 5$, arm length $N_m = 80$, and several values of the scaled gravitational field strength $G = 10^{-3}$, 10^{-2} , 10^{-1} , and 0.5 (left to right). See also movies in supporting information.

tions [55, 56]. MPC has been shown to provide valuable insight into a broad spectrum of nonequilibrium properties of systems such as polymers [10, 11, 60–65], colloids [49, 50, 66–69], vesicles and cells [20, 29, 70], and active particles [71–78].

We find a strong influence of fluid-mediated interactions on the nonequilibrium sedimentation and conformational properties of star polymers. The sedimentation coefficient and the radius of gyration of the star polymer exhibits a non-monotonic behavior. At intermediate field strengths, the coefficient increases with increasing field strength, assumes a maximum and decreases at large field strengths again. Thereby, the increase is more pronounced for star polymers with a larger arm number. The changes in the radius of gyration are strongly linked to those of the sedimentation coefficient, however, with the opposite trend, i.e., the radius of gyration decreases first and increases at large field strengths. Interestingly, the star polymers exhibit a trailing tail at high field strengths, with a few strongly stretched polymer arms.

The outline of paper is as follows. In section II, the star-polymer model, the coarse-grained description of the explicit solvent, and the interaction of the external field with the polymer are introduced. Section III presents results for the conformational and dynamical properties of the star polymers. All results are summarized and discussed in section IV.

II. MODELS

A. Star polymer

We consider a very dilute suspension of star polymers. A star polymer itself consists of f identical flexible linear polymers, which are linked at a common center by one of their ends. A polymer is modeled in a coarse-grained manner as a linear bead-spring chain of N_m beads of mass M , hence, the total number of beads are $N_p = fN_m + 1$. The bond potential is given by

$$V_B = \frac{k_s}{2} \sum_{\mu=1}^f \sum_{k=1}^{N_m-1} (|\mathbf{R}_{k+1}^\mu - \mathbf{R}_k^\mu| - l)^2 + \frac{k_s}{2} \sum_{\mu=1}^f (|\mathbf{R}_1^\mu - \mathbf{R}_0| - l_0)^2, \quad (1)$$

where \mathbf{R}_k^μ is the position of monomer k ($k \in \{1, \dots, N_m\}$) of arm μ ($\mu \in \{1, \dots, f\}$), l is the equilibrium bond length, and k_s denotes the spring constant. The bond length for the central bead \mathbf{R}_0 is l_0 . Excluded-volume interactions between non-bonded beads are taken into account by the repulsive, truncated, and shifted Lennard-Jones (LJ) potential [79]

$$V_{LJ} = 4\epsilon \sum_{\nu, \mu=1}^f \sum_{k, j=0}^{N_m} \left[\left(\frac{\sigma}{R_{kj}^{\nu\mu}} \right)^{12} - \left(\frac{\sigma}{R_{kj}^{\nu\mu}} \right)^6 + \frac{1}{4} \right] \times \Theta(2^{1/6}\sigma - \Delta R_{kj}^{\nu\mu}). \quad (2)$$

Here, $\Theta(x)$ is the Heaviside step function ($\Theta(x) = 0$ for $x < 0$ and $\Theta(x) = 1$ for $x \geq 0$). The distance between the monomers is $R_{kj}^{\nu\mu} = |\mathbf{R}_k^\nu - \mathbf{R}_j^\mu|$, with $\mathbf{R}_0^\nu \equiv \mathbf{R}_0$ ($\nu, \mu \in \{1, \dots, f\}$, $k, j \in \{0, \dots, N_m\}$). Self-interactions are excluded, i.e., $k \neq j$ for $\nu = \mu$.

Every star-polymer bead is exposed to the gravitational field $\hat{\mathbf{G}} = -\hat{G}\mathbf{e}_y$, where \mathbf{e}_y is the unit vector along the direction of the y -axis of the Cartesian reference system. Hence, it experiences the force

$$\mathbf{F}_G = M\hat{\mathbf{G}}. \quad (3)$$

In the sedimentation process, fluid is dragged along by a star polymer, which induces a fluid flow. In an experiment, this fluid is reflected by the confining container walls and induces a back-flow. To prevent a net fluid flow in our systems with periodic boundary conditions, we modify the equations of motion of the fluid in such a way that the total momentum of the system (fluid plus star polymer) is zero. By this requirement, fluid back-flow is introduced. This leads to the additional force on a bead

$$\mathbf{F}_f = -\frac{M^2 N_p}{MN_p + mN_s} \hat{\mathbf{G}}, \quad (4)$$

where m is the mass of the fluid particle, N_s is the total number of fluid particles, and MN_p is the total mass of a star polymer.

B. Multiparticle Collision Dynamics

The ambient fluid is described by the multiparticle collision dynamics (MPC) approach, an off-lattice, mesoscale, hydrodynamic simulation technique [54–56]. In this method, the fluid is represented by point particles with positions \mathbf{r}_i and velocities \mathbf{v}_i ($i = 1, \dots, N_s$). The particle dynamics proceeds in discrete steps, the streaming and collision step. During streaming, the fluid particles of mass m move ballistically in a closed system. However, the gravitational-field induced back-flow has to be taken into account, which yields the velocities and positions after streaming

$$\mathbf{v}_i(t+h) = \mathbf{v}_i(t) - \frac{MN_p}{MN_p + mN_s} \hat{\mathbf{G}}h, \quad (5)$$

$$\mathbf{r}_i(t+h) = \mathbf{r}_i(t) + h\mathbf{v}_i(t) - \frac{MN_s}{MN_p + mN_s} \hat{\mathbf{G}} \frac{h^2}{2}, \quad (6)$$

with the collision time h . In the collision step, the simulation box is partitioned into cubic cells of side length a to define the multiparticle collision environment. The solvent particles are sorted into these cells and their relative velocities, with respect to the center-of-mass velocity of the cell, are rotated around a randomly oriented axis by an angle α , i.e.,

$$\mathbf{v}_i(t+h) = \mathbf{v}_i(t) + (\mathbf{R}(\alpha) - \mathbf{I})(\mathbf{v}_i(t) - \mathbf{v}_{cm}(t)), \quad (7)$$

where \mathbf{R} is the rotation matrix, \mathbf{I} is the unit matrix, and $\mathbf{v}_{cm} = \sum_{j=1}^{N_c} \mathbf{v}_j / N_c$ is the center-of-mass velocity of the cell with N_c particles. In this stochastic process, mass, momentum, and energy are conserved. Momentum conservation ensures hydrodynamic behavior which emerges on larger length and time scales [55, 56, 80].

The interaction of the star polymers with the fluid is established during the collision step [56, 57, 65, 81]. Thereby, the bead velocities are rotated according to Eq. (7) similar to those of the fluid particles, with the center-of-mass velocity of the respective collision cell

$$\mathbf{v}_{cm}(t) = \frac{\sum_{i=1}^{N_c} m\mathbf{v}_i(t) + \sum_{k=1}^{N_c^m} M\mathbf{V}_k(t)}{mN_c + MN_c^m}. \quad (8)$$

Here, N_c^m is the number of beads in the considered cell. Thereby, momentum is redistributed between fluid and monomers and long-range correlations emerge [59].

In order to maintain a constant temperature and to remove the energy introduced by the external field, we apply the Maxwell-Boltzmann scaling (MBS) method, which yields a Maxwell-Boltzmann distribution of the fluid-particle velocities [82, 83]. In the MBS thermostat, the relative velocities—with respect to the center-of-mass velocity of a collision cell—of all particles within such a cell are scaled by a stochastic factor, leaving the dynamical properties of the system unaltered. The stochastic factor is determined from the Gamma distribution function of the kinetic energy of the particles in a cell.

C. Parameters

The dynamical behavior of the fluid depends on the various model parameters. The transport properties of the solvent are determined by the collision time h , the rotation angle α , the average number of particles $\langle N_c \rangle$ per cell [55, 56, 84–88], which corresponds to the fluid mass density $\rho_s = m\langle N_c \rangle / a^3$. Small collision times and a large number of average MPC particles result in fluid-like behavior with a high Schmidt number Sc . In our simulation, we choose parameters such that the transport of momentum due to collision dominates over diffusion. Explicitly, we use the collision time $h/\sqrt{ma^2/(k_B T)} = 0.1$, the rotation angle $\alpha = 130^\circ$, and $\langle N_c \rangle = 10$. These parameters correspond to the solvent viscosity $\eta_s = 8.7\sqrt{mk_B T}/a^4$, kinematic viscosity $\nu_s = \eta_s/\rho_s = 0.87\sqrt{a^2 k_B T/m}$, and the Schmidt number $Sc \approx 17$ [83].

We study the sedimentation behavior of star polymers with the polymer arm lengths $N_m = 10, 20, 40$, and 80. In order to achieve a comparable finite-size effect for the various polymer lengths on the dynamical quantities, we fix the ratio of the simulation box size along the field direction (y -axis) and the radius of gyration of the star polymer for the respective arm length. A polymer gets elongated in the field direction, thus the size of the simulation box along the field direction has to be larger than the polymer length. Explicitly, we apply the following extensions (L_x, L_y, L_z) of the simulation box for the various polymer lengths: $N_m = 80$, $L_x/a = 80$, $L_y/a = 200$, $L_z/a = 80$; $N_m = 40$, $L_x/a = 60$, $L_y/a = 130$, $L_z/a = 60$; $N_m = 20$ and $N_m = 10$, $L_x/a = 40$, $L_y/a = 90$, $L_z/a = 40$. Periodic boundary conditions are applied in all spatial directions. This corresponds to nearly 10^7 fluid particles for the polymer length $N_m = 80$ and nearly 10^5 fluid particles for $N_m = 10$. In general, $mN \gg MN_s$, hence the correction term for back flow (Eq. 4) is typically negligible. All the simulations are performed over a range of field strength $G = M\hat{G}l/k_B T$, where $10^{-4} \leq G < 10^{-1}$.

For the polymer, we use the Lennard-Jones parameters $\epsilon = k_B T$ and $\sigma/l = 0.8$. The parameters for the harmonic bonds are $l = a$ and $k_s/(k_B T/l^2) = 5000$. The mass of a bead is $M = 10m$. The size of the central bead and the bond lengths to the respective first bead of a polymer arm are twice as large as those of the polymers themselves. This is necessary to allow for a large number of arms to be connected to the central bead.

The velocity Verlet algorithm [79] is used to integrate Newton's equations of motion of the star polymer with the integration time step $h/20$.

For an efficient simulation of the system, we apply a hybrid procedure, where a graphics processing unit (GPU) is combined with a CPU. MPC is the most time-consuming part of our simulation. Hence, we divide the computational task into two parts. The equations of motion of the star polymer are always integrated on the

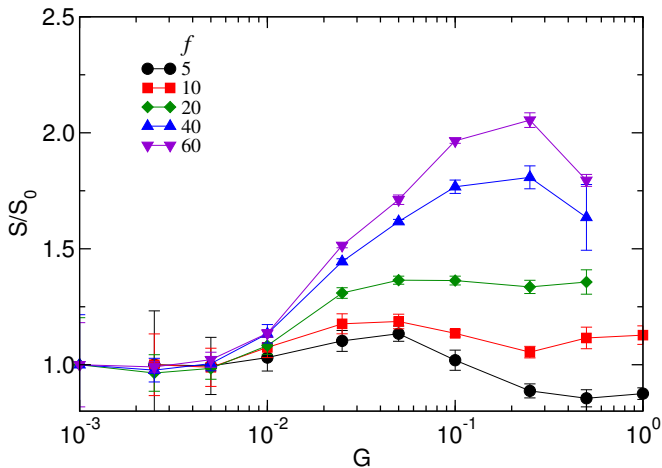


FIG. 2: Normalized sedimentation coefficients S/S_0 of star polymers with the indicated functionalities for the arm length $N_m = 80$ as a function of the external field $G = M\hat{G}l/(k_B T)$. S_0 is the sedimentation coefficient of the asymptotic weak-field limit.

CPU. The MPC dynamics is performed on a GPU. Since MPC streaming of the fluid particles as well as their collisional interactions are carried out independently, the fluid dynamics is highly parallelizable and can be managed in an efficient way on a GPU. After every MPC streaming step, velocities and positions of the monomers are transferred from the CPU to the GPU for the collisional interaction with the fluid particles. After the collision with fluid velocities are transferred back to the CPU for the integration of the bead equations of the solute. A detailed description of the GPU implementation of MPC is provided in Ref. [89].

III. RESULTS

A. Sedimentation Coefficient

Under the influence of the external field and in the stationary state, the star polymer drifts along the direction of the field, with a constant average velocity. Hence, the magnitude of the total external force $F_T = MN_p \hat{G}$ is equal to magnitude of the frictional force, i.e.,

$$MN_p \hat{G} = \gamma V_{cm}, \quad (9)$$

where γ is the total friction coefficient of the star polymer and $\mathbf{V}_{cm} = \sum_{i=1}^{N_s} \langle \mathbf{V}_i \rangle / N_s$ its center-of-mass velocity. The ratio of the center-of-mass velocity and the external force defines the sedimentation coefficient S , thus

$$S \equiv \frac{V_{cm}}{\hat{G}} = \frac{MN_p}{\gamma}. \quad (10)$$

Using Stokes relation, the friction coefficient ($\gamma = 6\pi\eta R_h$) is proportional to the hydrodynamic radius R_h of

the star polymer. With the approximation of the hydrodynamic radius by the radius of gyration R_g , for which scaling arguments yield the relation

$$R_g \sim l N_m^\nu f^{(1-\nu)/2}, \quad (11)$$

with the critical exponent $\nu \approx 0.6$ [46, 90, 91], the sedimentation coefficient should exhibit the scaling relation

$$S \sim N_m^{1-\nu} f^{(1+\nu)/2} \quad (12)$$

at least for unperturbed star polymers at low external forces. Our simulation studies of Ref. [92] on the diffusive dynamics of star polymers of various functionalities confirm approximately the dependence $R_g \sim f^{(1-\nu)/2}$, with $\nu \approx 0.63$ for the considered short polymers, but show a somewhat stronger dependence of the hydrodynamic radius on f , namely $R_h \sim f^{\hat{\delta}}$ with $\hat{\delta} = 0.29$ instead of 0.2. We like to mention that in the free draining limit, the friction coefficient is proportional to $N_m f$ and the sedimentation coefficient is independent of the star molecular weight.

Figure 2 displays sedimentation coefficients for various functionalities as function of the scaled strength $G = M\hat{G}l/k_B T$ of the external field. Note, l corresponds to the Kuhn length of the polymer. The curves are normalized by the respective asymptotic sedimentation coefficient S_0 in the limit of vanishing field. As expected, the sedimentation coefficient is independent of G in the linear response regime for all functionalities. To achieve accurate results, we have generated nearly 50 independent data sets for every f in the weak-field limit, because here thermal fluctuations are strong and the drift is weak. In an intermediate regime, S/S_0 increases with increasing G , passes through a maximum and decreases again. Since we are limited in the range of applicable forces, we cannot extend our studies to large G and, hence, cannot comment on the behavior for asymptotically large values. However, we observe a strong dependence on the functionality. Thereby, S/S_0 increases with increasing f for intermediate field strengths and the maximum shifts to larger G . This is certainly related to considerable conformational changes of the star polymer as illustrated in Fig. 1.

The dependence of the sedimentation coefficient S_0 on the arm length and number is shown in Fig. 3. The values of S_0 for various N_m and f are obtained in the linear response regime in the weak field limit. In this regime, S_0 is independent of G . In accord with the scaling prediction of Eq. (12), S_0 increases with increasing N_m and f , respectively. Thereby, we find $S_0 \sim N_m^{0.37}$ in close agreement with Eq. (12) for $\nu \approx 0.63$. The latter value is consistent with various simulation studies of equilibrium and nonequilibrium properties of star polymers for the considered arm lengths [49, 51, 68, 92]. For the dependence of S_0 in f , we find the power law $S_0 \sim f^{\hat{\delta}}$, with $\hat{\delta} \approx 0.4$ independent of polymer length. However, $\hat{\delta}$ is significantly smaller than the value predicted by scaling considerations [Eq. (12)], which is 0.82. Even if we consider

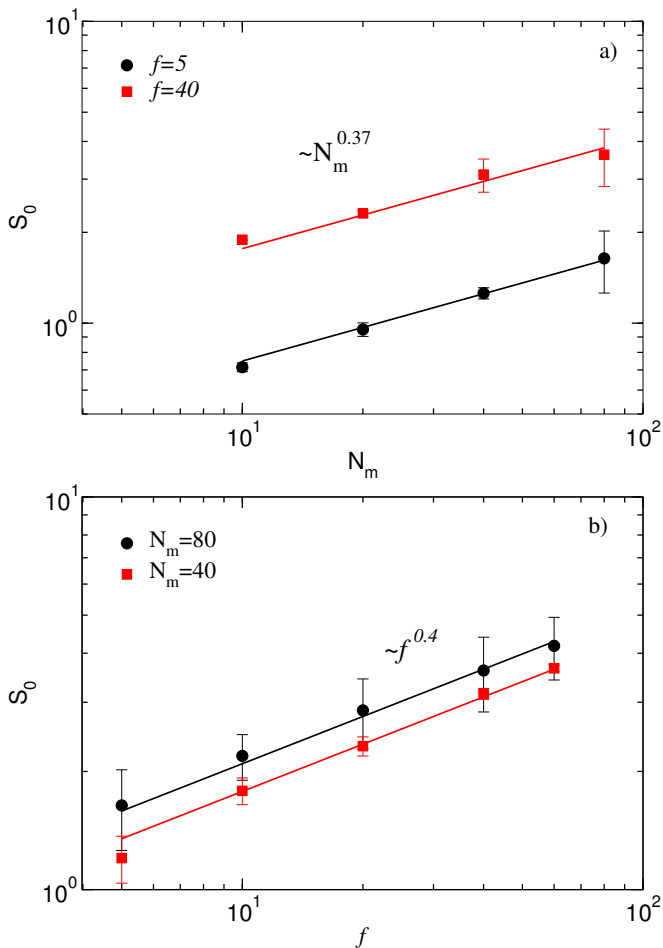


FIG. 3: a) Dependence of the sedimentation coefficient S_0 on the length of polymer arms for $f = 5$ and $f = 40$. The solid lines illustrate the power-law dependence $S_0 \sim N_m^{1-\nu}$, where $\nu \approx 0.63$. b) Dependence of the sedimentation coefficient S_0 on the number of polymer arms f for the arm lengths $N_m = 40$ and $N_m = 80$. The solid lines are the power-law fits $S_0 \sim f^\delta$, with $\delta \approx 0.4$.

the somewhat stronger dependence $R_h \sim f^{0.29}$ on functionality, the value $\delta = 0.4$ is significantly smaller than the theoretical prediction. The origin of the discrepancy remains to be resolved, but back flow might influence the hydrodynamic interactions between the beads.

Figure 4 displays scaled sedimentation coefficient S/S_0 for the polymer lengths $N_m = 10, 20, 40$, and 80 , and the two different functionalities $f = 5$ and 40 as function of the Weissenberg number Wi . The Weissenberg number is defined as follows. At weak external fields, a star polymer experiences a shear force on its surface during sedimentation, which gives rise to the shear rate $\dot{\gamma} \sim V_{cm}/R_g$. Within the blob model of a star polymer [46, 47], this leads to the scaling relation for $\dot{\gamma}$ in terms of the arm length and functionality

$$\dot{\gamma} \sim \hat{G} N_m^{1-2\nu} f^\nu. \quad (13)$$

The relaxation of a polymer arm is dominated by the

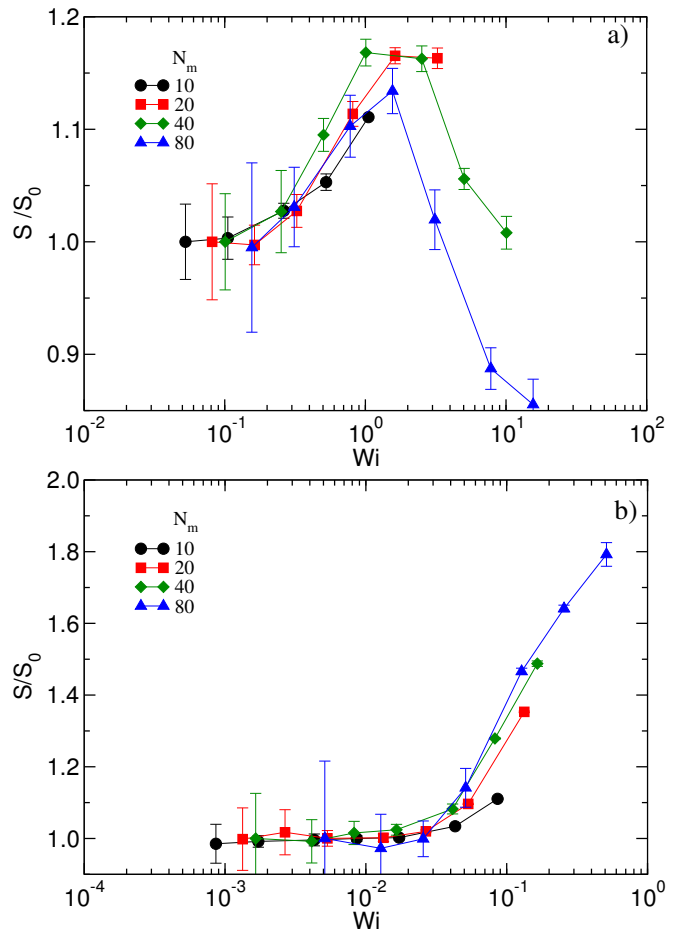


FIG. 4: Scaled sedimentation coefficients S/S_0 of star polymers with the indicated arm lengths as function of the Weissenberg number Wi (Eq. (14)) for the arm numbers a) $f = 5$ and b) 40 .

relaxation of its largest blob [47] and, hence, we define a Weissenberg number via $Wi = \dot{\gamma}\tau_B$, with the blob relaxation time τ_B . In the presence of hydrodynamic interactions, $\tau_B \sim R_B^3$, where R_B is the blob radius. The latter scales as $R_B \sim R_g f^{-1/2} \sim N_m^\nu f^{-1/2}$ with arm length and functionality [47]. Thus, we finally obtain the scaling relation for the Weissenberg number

$$Wi \sim \hat{G} N_m^{1+\nu} f^{\nu-3/2}. \quad (14)$$

In the following, we present the sedimentation coefficient as function of the Weissenberg number, taking Wi as $Wi = \hat{G} N_m^{1+\nu} f^{\nu-3/2}$. As displayed in Fig. 4, a reasonable scaling of the curves for various arm lengths is only achieved for the functionality $f = 40$ and longer arms. The predicted dependence on functionality is not reproduced by the simulations. This is not surprising, since the obtained scaling in Fig. 3 b) deviates from the simple scaling prediction.

As with increasing functionality, the ratio of S/S_0 increases with increasing external field strength in the non-linear response regime. This increase is consistent with

simulation results of linear polymers [44]. The onset of the non-linear regime is reasonably well captured by the prediction (14). As displayed in Fig. 4 b), in particular for the longer polymer arms, the sedimentation coefficient shows a non-monotonic dependence on the external field; it passes through a maximum value and then decreases again with increasing Wi . We expect a similar behavior for the shorter polymers, however, for them, we cannot reach large field strengths without violating limitations of the MPC method, e.g., small Mach numbers. The influence of the external field seems to be more pronounced for star polymers with a larger number of arms. Over the accessible range of field strengths, the values S/S_0 for star polymers of functionality $f = 40$ are always higher than their linear-response-regime values (Fig. 4b)), whereas the values of S/S_0 for $f = 5$ are below the linear-response-regime values (Fig. 4a)).

Considering the sedimentation velocities and the sizes of the star polymers, a remark on the Reynolds number is in order. Taking characteristic values for the sedimentation velocity and the radius of gyration, the Reynolds number Re is $Re = 2S_0\hat{G}R_{g0}/\nu \approx 10G$ for $S_0 = 3$ and $R_{g0} = 15a$. Hence, the Reynolds number is larger than unity for $G \gtrsim 0.1$. This implies that the observed saturation or weak decrease of the sedimentation coefficient (Fig. 2) appears for Reynolds numbers larger than unity. A priori, the effect of the Reynolds number on S in this regime is not evident. A comparison of our results with those of Refs. [41, 44] at zero Reynolds number for linear and ring polymers shows qualitative agreement— S increases first with increasing G and decreases again at larger G . Thereby, in Refs. [41, 44] larger G values are considered. Hence, from a qualitative point of view, we consider our results for star polymers as representative and expect a similar behavior for smaller Reynolds numbers. This is supported by Fig. 5, showing a non-turbulent flow field of a sedimenting star even at $Re > 1$. In any case, the simulation results for the larger G values reflect the sedimentation behavior of star polymers at the respective Reynolds numbers.

B. Structural Properties

Strong external fields induce large-scale conformational changes of the ultra-soft colloids, as illustrated in Fig. 1 for our star polymers. In-order to characterize these conformational changes, we compute the radius-of-gyration tensor, which is defined as

$$G_{\alpha\beta} = \frac{1}{N_s} \left\langle \sum_{i=1}^{N_s} \Delta R_{i\alpha} \Delta R_{i\beta} \right\rangle. \quad (15)$$

Here, $\Delta R_{i\alpha}$ is the position of the i^{th} bead relative to the star center-of-mass, and $\alpha, \beta \in \{x, y, z\}$. In the limit of a vanishing field, a star polymer is isotropic and all the diagonal components are equal, i.e., $G_{\alpha\alpha} = G_{\alpha\alpha}^{00} =$

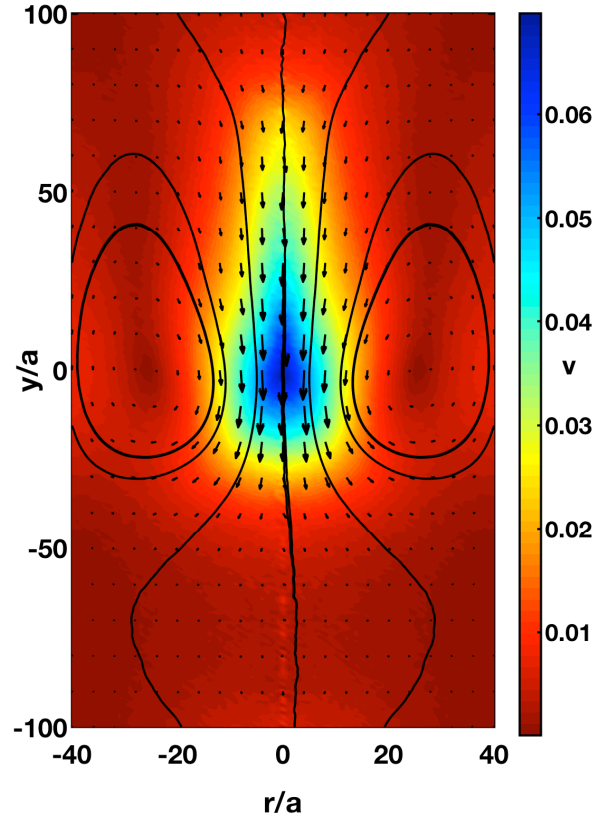


FIG. 5: Flow field of a star polymer in the laboratory reference frame for the arm length and number $N_m = 80$, $f = 60$, and field strength $G = 0.5$. The coordinate r is the radial distance with respect to sedimentation direction (y axis). The star polymer drags along fluid, which is indicated by the velocity-field vectors and solid black line. The flow lines in the head region reflect the recirculation of fluid [41]. Despite the strong field corresponding to Reynolds numbers larger than unity, the flow is laminar.

$R_{g0}^2/3$, where R_{g0} is the equilibrium radius of gyration [Eq. (11)].

Figure 6 shows normalized mean square radii of gyration R_g^2 and its components R_{gL}^2 and R_{gT}^2 along and transverse to the external field, respectively, as function of the field strength G for various functionalities. In the linear response regime, $G \lesssim 2 \times 10^{-4}$, the size of a colloid is equal to its unperturb equilibrium value. In an intermediate regime, R_g^2 decreases with increasing field strength. This compression of the ultra-soft colloid is more pronounced for high functionality star polymers. Both, the transverse and longitudinal components R_{gL}^2 and R_{gT}^2 are reduced. In the case of $f = 10$, mainly R_{gT}^2 decreases with increasing G . We attribute this reduction in colloid size to hydrodynamics. The front of the star polymer experience a drag force, which causes a compression. In addition, the flow surrounding the non-draining

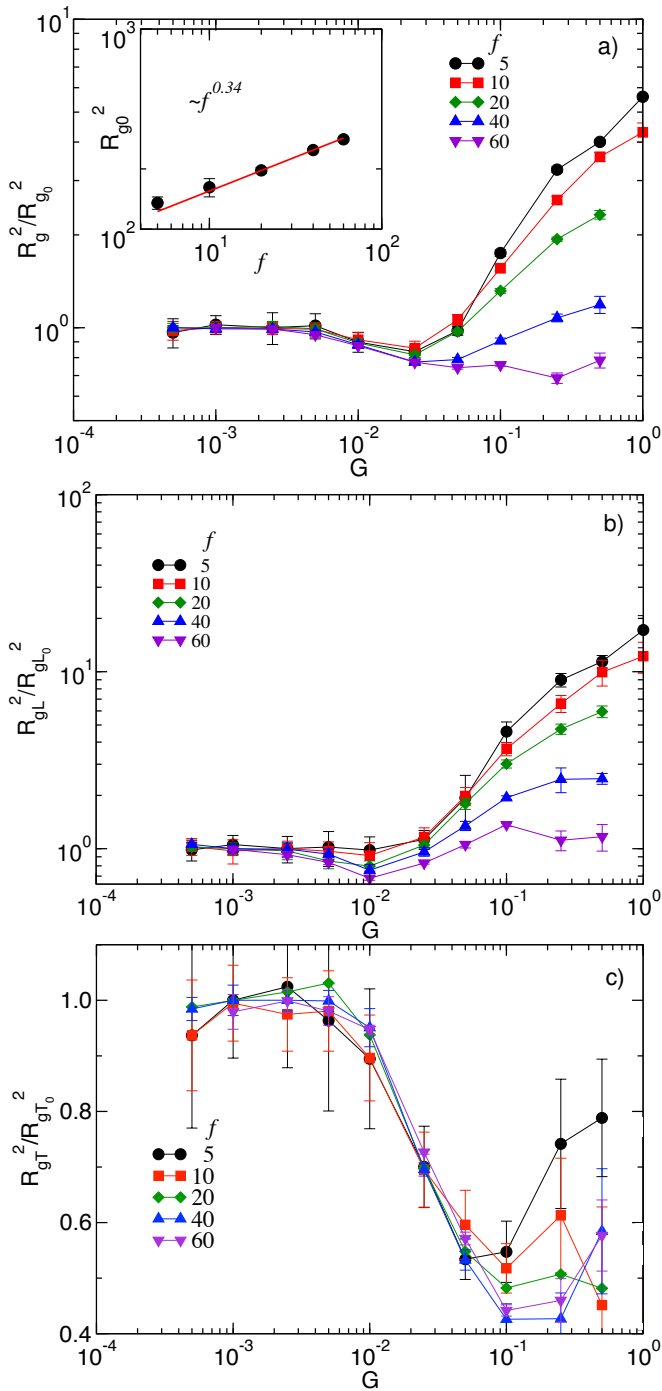


FIG. 6: a) Overall radii of gyration of star polymers and their components b) along and c) perpendicular to the field as function of the external field for the indicated functionalities and the arm length $N_m = 80$. The inset in a) shows the dependence of the equilibrium radius of gyration R_{g0}^2 on the functionality f .

colloid exerts an inward force, which strongly affects R_{gT} . This is similar to the flow field of a linear polymer as discussed in Ref. [41]. Above a functionality-dependent-field strength, the longitudinal component of the radius

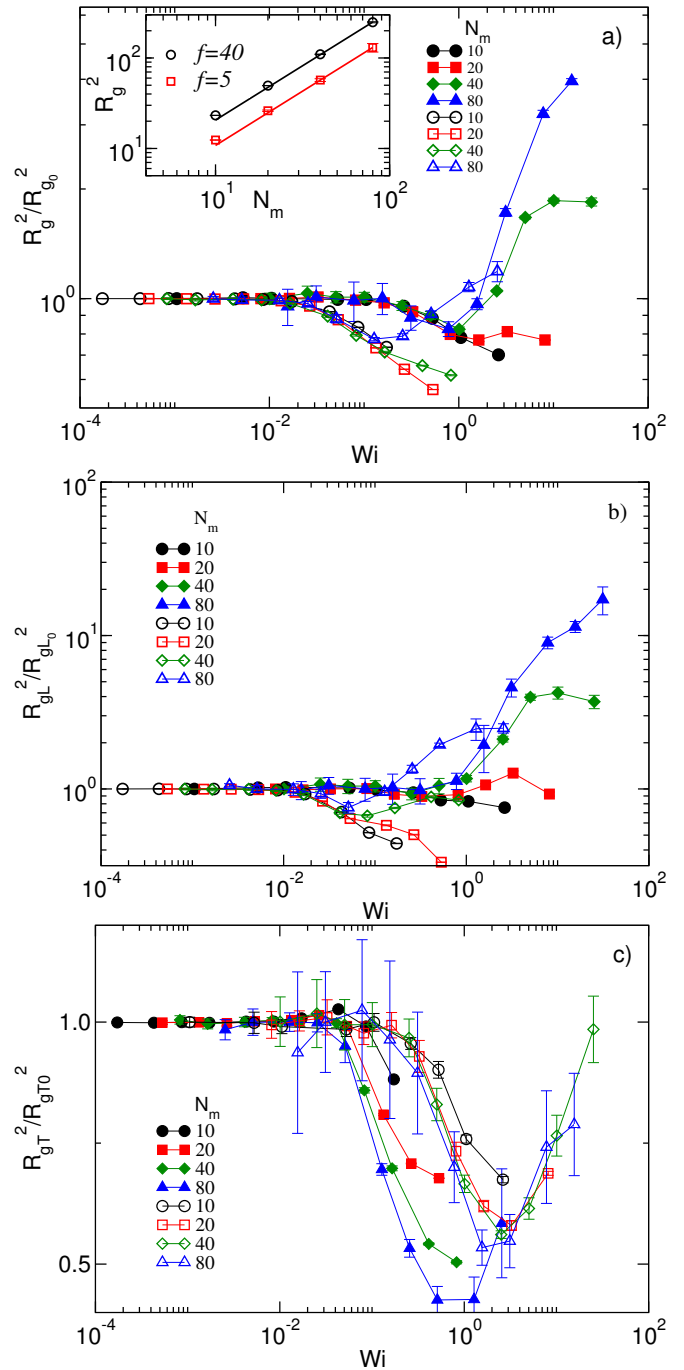


FIG. 7: a) Overall radii of gyration of star polymers and their components b) along and c) perpendicular to the field as function of Wi for the indicated arm lengths. Open symbols correspond to $f = 40$ and closed symbols to $f = 5$. The inset in a) shows the dependence of the equilibrium radius of gyration $R_{g0}^2 \sim N_m^{2\nu}$ on the arm length N_m , where $\nu = 0.63$.

of gyration along with R_g increases with increasing G . This increase is most pronounced for low-functionality star polymers. As illustrated in Fig. 1, in the limit of high fields, polymer arms are stretched, lag behind the center of the star polymer and yield an increase of its radius of

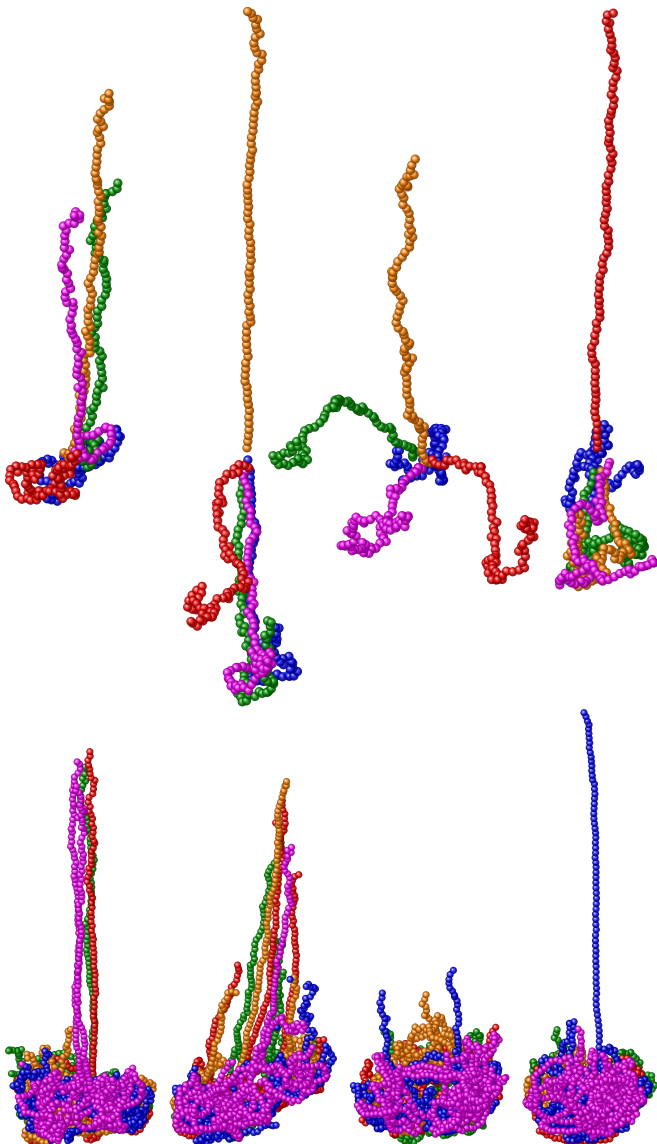


FIG. 8: Snapshots of sedimenting star polymers for different times. The arm length is $N_m = 80$, the strength of the external field $G = 0.5$, and the arm number $f = 5$ (top) and $f = 40$ (bottom), respectively. See also movies in supporting information.

gyration. In this regime, the top-bottom symmetry of the star polymer is broken. Polymer arms in front of the star-polymer center are compressed, whereas arms behind the center are stretched significantly. This implies that the monomer density in the front core is higher and therefore also the gravitational pull. A similar anisotropic shape appears for other soft colloidal objects in a gravitational field, such as red blood cells [37]. Within the accuracy of our simulations, the components of the radius of gyration tensor seem to approach constant values at large field strengths. (Note the pronounced fluctuations (error bars) of R_{gT}^2 at larger G values due to large-scale shape changes of the head (cf. Fig. 8).) We attribute

this, on the one hand, to the maximal possible stretching of the polymer arms and, on the other hand, a saturation of the compression of the major part of the star polymer by the fluid flow. The latter is to be expected for the transverse component of the radius of gyration, since excluded-volume interactions allow for a minimal size only.

The inset of Fig. 6 a) shows the dependence of the equilibrium radius of gyration on the functionality for the arm length $N_m = 80$. The solid line indicates the power-law dependence $R_g^2 \sim f^{1-\nu}$, with the exponent $\nu \sim 0.63$, which is consistent with the theoretical expectation according to Eq. (11).

The dependence of the star polymer radius of gyration on the polymer arm length is displayed in Fig. 7 for $f = 5$ and $f = 40$ as function of the Weissenberg number. Here, we find good agreement between the curves for the various arm lengths as long as flow leads to a shrinkage of the star polymers. The appearance of strongly extended tails breaks the universality. Again, the predicted scaling relation (14) fails to describe the obtained functionality dependence. For short arm lengths, we observe a monotonic decrease of the star polymer size and a crossover to a non-monotonic behavior for longer arms. In case of short polymers ($N_m \lesssim 20$), the radius of gyration and its components R_{gL} and R_{gT} always decreases for all Wi and both functionalities over the considered range of external field strengths. The size of the longer-arm star polymers increases again at higher field strengths due to the appearance of strongly stretched polymers. We expect such an increase for all polymer lengths. There is a critical field strength, which has to be exceeded to achieve the increase in size. This critical field strength depends on the arm length and the functionality and seems to be different for the longitudinal and transverse part of the radius of gyration. Whereas R_{gL}^2 clearly increases for $N_m \gtrsim 40$ and $Wi > 1$ ($f = 5$) ($Wi > 10^{-1}$, ($f = 40$)), the respective values for the other arm lengths still decrease. The transverse components of the radii of gyration behave rather similarly, and R_{gT}^2 increases again for $Wi \gtrsim 1$. Thereby, the relative change in R_g^2 for the fewer-arm stars is always larger than that of the higher functionality stars.

The star-polymer structure is highly dynamic. Although the overall shape is rather stable for a long time with the majority of polymer arms close to the center of mass and an extended trailing tail [41, 44], the individual polymers undergo considerable conformational changes. This is illustrated in Figure 8. For a movie, see in supporting information. The emergence of an extended tail leads to an increase of the radii of gyration R_g^2 and R_{gL}^2 . This increase is more pronounced for low-functionality star polymers as reflected in Figs. 6 and 7. For high-functionality star polymers, the relative weight of the small number of arms ($\lesssim 5$) in the trailing tail is less important than for low-functionality star polymers. More remarkable is the increase of R_{gT} at large field strengths. Here, the flow field seems to perturb the lower-field flow-

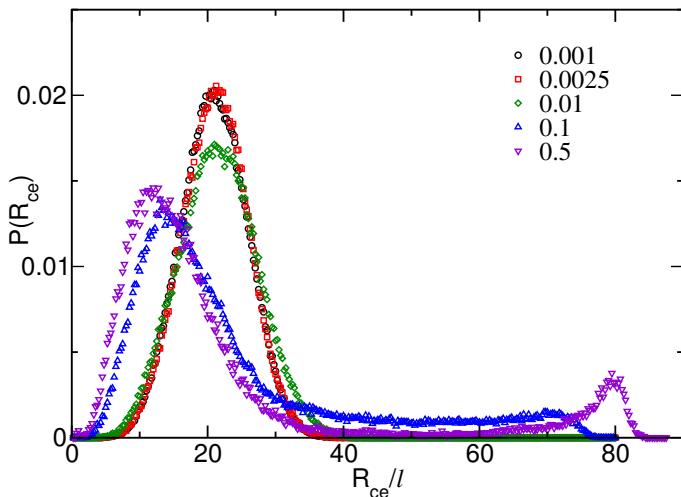


FIG. 9: Normalized probability distribution function $P(R_{ce})$ of the center-to-end distance of polymers arms of length $N_m = 80$ and the star-polymer functionality $f = 40$ for various field strength G (as indicated).

induced compact structure and implies larger conformational changes of the polymers.

We have shown that the symmetry of the colloidal structure of the star polymer is broken in the limit of high field strengths. The asymmetric distribution of polymer arms in the high-field limit can be qualitatively illustrated by the probability distribution of the center-to-end distance of the polymer arms. As an example, Fig. 9 shows the normalized probability distribution function $P(R_{ce})$ of the center-to-end distance of polymer arms for various field strengths. In the weak-field limit, the distribution of the center-to-end distance exhibits a peak at $R_{ce}/l \approx 20$ corresponding to the equilibrium value. With increasing G , the peaks shifts toward smaller values of the center-to-end distance and broaden substantially for large values of G due to compressive force. At the same time, the probability for extended polymer arms increases. This signifies that on average a few arms are stretched while the majority of arms is compressed. In the limit of strong fields, the distribution function exhibits two peaks, at $R_{ce}/l \approx 10$ and $R_{ce}/l \approx 80$. The smaller peak at $R_{ce}/l \approx 80$ corresponds to nearly fully stretched arms. The height of the peak, smaller than the small-distance peak, reflects that only a few arms are strongly stretched, but that this stretched conformations are rather stable and persistent. Due to fluctuations, stretched arms collapse and are replaced by others. Thereby, the collapse process is very fast, which leads to a low probability in the range $40 \lesssim R_{ce}/l < 70$.

IV. SUMMARY AND CONCLUSIONS

We have investigated the steady-state sedimentation properties of ultra-soft colloids (star polymers) via hybrid

mesoscale computer simulations. We find that the mobility of the ultra-soft colloid exhibits a non-monotonic dependence on the external field strength \hat{G} . The sedimentation coefficient reaches a maximum value at an intermediate range of \hat{G} . Thereby, for star polymers with fewer arms, the maximum appears at smaller field strengths and the sedimentation coefficient assumes smaller values in the high-field regime than the asymptotic value in the limit of vanishing field. The non-monotonic behavior of the sedimentation coefficient is related to flow-induced conformational changes of the star polymers. The increase of the sedimentation coefficient follows by a decrease of the radius of gyration. In the limit of high field strengths, the mobility decreases due to the stretching of various polymer arms along the field direction. Hence, the nonequilibrium dynamical properties of the star polymers are tightly linked with their structure. In the limit of strong external fields, the star polymers are no longer spherically symmetric. They rather exhibit a compact advancing structure, which is followed by a trailing tail of a few polymer arms. The number of polymers in the tail strongly fluctuate and their numbers depends on the functionality.

The nonmonotonic behavior of the dynamical and structural properties appears in our simulations for $Re \gtrsim 1$. Nevertheless, we expect a very similar behavior for Reynolds numbers significantly smaller than unity. Our expectation is supported by the zero-Reynolds number simulations of Refs. [41, 44], where linear and ring polymers exhibits a qualitatively similar behavior.

For weak fields, the star polymers sediment maintaining their equilibrium shape and the sedimentation coefficient exhibits the arm length and functionality dependence $S_0 \sim N_m^{1-\nu} f^\delta$, with $\delta \approx 0.4$. An additional speed up with increasing arm number is obtained for stars in the non-linear regime over a certain range of gravitational constants, with trailing polymer arms. An additional factor is also obtained in the non-linear regime for different arm lengths. However, the increase or even decrease of S is less pronounced by varying the arm length than by varying the functionality. Hence, non-linear effects can enhance sedimentation and promote separation of star polymers of different sizes.

V. ACKNOWLEDGEMENT

Financial support by the Deutsche Forschungsgemeinschaft (DFG) through the Collaborative Research Center "Physics of Colloidal Dispersions in External Fields" (SFB TR6), by the EU through the Collaborative Research Project "NanoDirect" (NMP4-SL-2008-213948), and the EU through FP7-Infrastructure ESMI (Grant 262348) are gratefully acknowledged. The authors gratefully acknowledge the computing time granted on the supercomputers at Jülich Supercomputing Centre (JSC).

Appendix A: Fluid backflow

The equation of motion of a monomer of the star polymer in the laboratory reference frame (indicated by a prime) is given by

$$M\ddot{\mathbf{R}}_k'^\mu = \mathbf{F}_k'^\mu + M\hat{\mathbf{G}}, \quad (\text{A1})$$

where the $\mathbf{F}_k'^\mu$ are intramolecular forces following from the potential (1) and (2). The center-of-mass velocity of the total system, star polymer plus MPC fluid, is then

$$M_{tot}\dot{\mathbf{r}}_{cm}' = N_p M\hat{\mathbf{G}}, \quad (\text{A2})$$

with $M_{tot} = N_p M + N_s m$ and

$$\mathbf{r}'_{cm} = \frac{1}{M_{tot}} \left(\sum_{k,\mu} M\mathbf{R}_k'^\mu + \sum_i m\mathbf{r}'_i \right). \quad (\text{A3})$$

Introducing the coordinates $\mathbf{R}_k^\mu = \mathbf{R}_k'^\mu - \mathbf{r}'_{cm}$ and $\mathbf{r}_i = \mathbf{r}'_i - \mathbf{r}'_{cm}$ of the monomer and fluid particle positions with respect to the total center-of-mass implies

$$\sum_{k,\mu} M\ddot{\mathbf{R}}_k^\mu + \sum_i m\ddot{\mathbf{r}}_i = 0, \quad (\text{A4})$$

i.e., conservation of the total moment in the center-of-mass reference frame. We set this moment to zero initially. From Eq. (A1), we obtain then

$$M\ddot{\mathbf{R}}_k^\mu = \mathbf{F}_k^\mu + M\hat{\mathbf{G}} + \mathbf{F}_f, \quad (\text{A5})$$

with

$$\mathbf{F}_f = -\frac{M^2 N_p}{M N_p + m N_s} \hat{\mathbf{G}}. \quad (\text{A6})$$

Similarly, we obtain for the fluid particles

$$m\ddot{\mathbf{r}}_i = \frac{m}{M} \mathbf{F}_f. \quad (\text{A7})$$

Supplementary Material

Two movie files and a figure are provided to illustrate the star polymer conformations. S1: A sedimenting star polymer is shown w.r.t. to its centre bead for the functionality $f = 5$ and $G = 0.5$ at the arm length $N_m = 80$. S2: The same set of parameters are applied as in S1, except the number of arms is $f = 40$.

-
- [1] R. G. Larson, *The structure and rheology of complex fluids* (Oxford University Press, Oxford, NY, 1999).
- [2] R. B. Bird, R. C. Armstrong, and O. Hassager, *Dynamics of polymeric liquids: Fluid mechanics* (Wiley, New York, 1987), 2nd ed.
- [3] D. E. Smith, H. P. Babcock, and S. Chu, *Science* **283**, 1724 (1999).
- [4] P. LeDuc, C. Haber, G. Boa, and D. Wirtz, *Nature* **399**, 564 (1999).
- [5] M. Kröger, *Phys. Rep.* **390**, 453 (2004).
- [6] C. M. Schroeder, R. E. Teixeira, E. S. G. Shaqfeh, and S. Chu, *Phys. Rev. Lett.* **95**, 018301 (2005).
- [7] S. Gerashchenko and V. Steinberg, *Phys. Rev. Lett.* **96**, 038304 (2006).
- [8] R. G. Winkler, *Phys. Rev. Lett.* **97**, 128301 (2006).
- [9] R. M. Jendrejack, D. C. Schwartz, J. J. de Pablo, and M. D. Graham, *J. Chem. Phys.* **120**, 2513 (2004).
- [10] R. Chelakkot, R. G. Winkler, and G. Gompper, *EPL* **91**, 14001 (2010).
- [11] R. Chelakkot, R. G. Winkler, and G. Gompper, *Phys. Rev. Lett.* **109**, 178101 (2012).
- [12] D. Steinhäuser, S. Köster, and T. Pfohl, *ACS Macro Lett.* **1**, 541 (2012).
- [13] M. Harasim, B. Wunderlich, O. Peleg, M. Kröger, and A. R. Bausch, *Phys. Rev. Lett.* **110**, 108302 (2013).
- [14] T. Pakula, D. Vlassopoulos, G. Fytas, and J. Roovers, *Macromolecules* **31**, 8931 (1998).
- [15] D. Vlassopoulos, G. Fytas, T. Pakula, and J. Roovers, *J. Phys. Condens. Matter* **13**, R855 (2001).
- [16] A. Nikoubashman and C. N. Likos, *Macromolecules* **43**, 1610 (2010), URL <http://dx.doi.org/10.1021/ma902212s>.
- [17] D. Vlassopoulos and M. Cloitre, *Curr. Opin. Colloid Interface Sci.* **19**, 561 (2014).
- [18] R. G. Winkler, D. A. Fedosov, and G. Gompper, *Curr. Opin. Colloid Interface Sci.* **19**, 594 (2014), URL <http://www.sciencedirect.com/science/article/pii/S1359029414000922>.
- [19] S. R. Keller and R. Skalak, *Journal of Fluid Mechanics* **120**, 27 (1982).
- [20] H. Noguchi and G. Gompper, *Phys. Rev. Lett.* **93**, 258102 (2004).
- [21] V. Kantsler and V. Steinberg, *Physical review letters* **96**, 036001 (2006).
- [22] C. Misbah, *Physical review letters* **96**, 028104 (2006).
- [23] V. Lebedev, K. Turitsyn, and S. Vergeles, *Physical review letters* **99**, 218101 (2007).
- [24] P. M. Vlahovska and R. S. Gracia, *Physical Review E* **75**, 016313 (2007).
- [25] H. Zhao and E. S. Shaqfeh, *Journal of Fluid Mechanics* **674**, 578 (2011).
- [26] D. Abreu, M. Levant, V. Steinberg, and U. Seifert, *Advances in colloid and interface science* **208**, 129 (2014).
- [27] A. Lamura and G. Gompper, *EPL (Europhysics Letters)* **102**, 28004 (2013).
- [28] M. Abkarian, M. Faivre, and A. Viallat, *Physical Review Letters* **98**, 188302 (2007).
- [29] H. Noguchi and G. Gompper, *Proceedings of the National Academy of Sciences of the United States of America* **102**, 14159 (2005).

- [30] B. Kaoui, G. Biroso, and C. Misbah, *Physical review letters* **103**, 188101 (2009).
- [31] J. Dupire, M. Socol, and A. Viallat, *Proceedings of the National Academy of Sciences* **109**, 20808 (2012).
- [32] I. V. Pivkin and G. E. Karniadakis, *Physical Review Letters* **101**, 118105 (2008).
- [33] J. L. McWhirter, H. Noguchi, and G. Gompper, *Proceedings of the National Academy of Sciences USA* **106**, 6039 (2009).
- [34] G. Tomaiuolo, M. Simeone, V. Martinelli, B. Rotoli, and S. Guido, *Soft Matter* **5**, 3736 (2009).
- [35] D. A. Reasor, J. R. Clausen, and C. K. Aidun, *International Journal for Numerical Methods in Fluids* **68**, 767 (2012).
- [36] D. A. Fedosov, M. Peltomäki, and G. Gompper, *Soft matter* **10**, 4258 (2014).
- [37] M. Peltomaki and G. Gompper, *Soft Matter* **9**, 8346 (2013), URL <http://dx.doi.org/10.1039/C3SM50592H>.
- [38] S. E. Harding, A. J. Rowe, and J. C. Horton, *Analytical Ultracentrifugation in Biochemistry and Polymer Science; Royal Society of Chemistry* (Cambridge, UK, 1993).
- [39] T. M. Laue and W. F. Stafford, *Annu. Rev. Biophys. Biomol. Struct.* **28**, 75 (1993).
- [40] K. B. Abbitt and G. B. Nash, *Am. J. Physiology* **285**, H229 (2003).
- [41] X. Schlagberger and R. R. Netz, *Macromolecules* **41**, 1861 (2008), URL <http://dx.doi.org/10.1021/ma070947m>.
- [42] B. Zimm and V. Schumaker, *Biophys. Chem.* **5**, 265 (1976).
- [43] D. Ertaş and M. Kardar, *Phys. Rev. E* **48**, 1228 (1993), URL <http://link.aps.org/doi/10.1103/PhysRevE.48.1228>.
- [44] X. Schlagberger and R. R. Netz, *Phys. Rev. Lett.* **98**, 128301 (2007), URL <http://link.aps.org/doi/10.1103/PhysRevLett.98.128301>.
- [45] J. Stellbrink, J. Allgair, M. Monkenbusch, D. Richter, A. Lang, C. Likos, M. Watzlawek, H. Löwen, G. Ehlers, and P. Schleger, in *Trends in Colloid and Interface Science XIV*, edited by V. Buckin (Springer Berlin Heidelberg, 2000), vol. 115 of *Progress in Colloid and Polymer Science*, pp. 88–92.
- [46] G. S. Grest, K. Kremer, and T. A. Witten, *Macromolecules* **20**, 1376 (1987).
- [47] G. S. Grest, K. Kremer, S. T. Milner, and T. A. Witten, *Macromolecules* **22**, 1904 (1989).
- [48] M. Ripoll, R. G. Winkler, and G. Gompper, *Phys. Rev. Lett.* **96**, 188302 (2006).
- [49] S. P. Singh, D. A. Fedosov, A. Chatterji, R. G. Winkler, and G. Gompper, *J. Phys.: Condens. Matter* **24**, 464103 (2012).
- [50] S. P. Singh, R. G. Winkler, and G. Gompper, *Phys. Rev. Lett.* **107**, 158301 (2011).
- [51] S. P. Singh, A. Chatterji, G. Gompper, and R. G. Winkler, *Macromolecules* **46**, 8026 (2013).
- [52] S. Gupta, S. Kundu, J. Stellbrink, L. Willner, J. Allgair, and D. Richter, *J. Phys: Condens. Matter* **24**, 464102 (2012).
- [53] J. Sablic, M. Praprotnik, and R. Delgado-Buscalioni, *Soft Matter* **13**, 4971 (2017), URL <http://dx.doi.org/10.1039/C7SM00364A>.
- [54] A. Malevanets and R. Kapral, *J. Chem. Phys.* **110**, 8605 (1999).
- [55] R. Kapral, *Adv. Chem. Phys.* **140**, 89 (2008).
- [56] G. Gompper, T. Ihle, D. M. Kroll, and R. G. Winkler, *Adv. Polym. Sci.* **221**, 1 (2009).
- [57] A. Malevanets and J. M. Yeomans, *Europhys. Lett.* **52**, 231 (2000).
- [58] C.-C. Huang, G. Gompper, and R. G. Winkler, *J. Phys.: Condens. Matter* **24**, 284131 (2012).
- [59] C. C. Huang, G. Gompper, and R. G. Winkler, *J. Chem. Phys.* **138**, 144902 (2013).
- [60] N. Kikuchi, A. Gent, and J. M. Yeomans, *Eur. Phys. J. E* **9**, 63 (2002), URL <http://dx.doi.org/10.1140/epje/i2002-10056-6>.
- [61] M. A. Webster and J. M. Yeomans, *J. Chem. Phys.* **122**, 164903 (2005).
- [62] J. F. Ryder and J. M. Yeomans, *J. Chem. Phys.* **125**, 194906 (2006).
- [63] S. Frank and R. G. Winkler, *EPL* **83**, 38004 (2008).
- [64] S. Frank and R. G. Winkler, *J. Chem. Phys.* **131**, 234905 (2009).
- [65] C.-C. Huang, R. G. Winkler, G. Sutmann, and G. Gompper, *Macromolecules* **43**, 10107 (2010).
- [66] J. T. Padding and A. A. Louis, *Phys. Rev. Lett.* **93**, 220601 (2004).
- [67] M. Ripoll, R. G. Winkler, and G. Gompper, *Phys. Rev. Lett.* **96**, 188302 (2006).
- [68] D. A. Fedosov, S. P. Singh, A. Chatterji, R. G. Winkler, and G. Gompper, *Soft Matter* **8**, 4109 (2012).
- [69] A. Nikoubashman and C. N. Likos, *J. Chem. Phys.* **133**, 074901 (2010).
- [70] J. L. Mcwhirter, H. Noguchi, and G. Gompper, *Proc. Natl. Acad. Sci. USA* **106**, 6039 (2009).
- [71] Y.-G. Tao and R. Kapral, *Soft Matter* **6**, 756 (2010).
- [72] A. Zöttl and H. Stark, *Phys. Rev. Lett.* **108**, 218104 (2012).
- [73] J. Elgeti and G. Gompper, *Proc. Natl. Acad. Sci. USA* **110**, 4470 (2013).
- [74] S. Y. Reigh, R. G. Winkler, and G. Gompper, *Soft Matter* **8**, 4363 (2012).
- [75] M. Theers and R. G. Winkler, *Soft Matter* **10**, 5894 (2014), URL <http://dx.doi.org/10.1039/C4SM00770K>.
- [76] M. Theers, E. Westphal, G. Gompper, and R. G. Winkler, *Soft Matter* **12**, 7372 (2016), URL <http://dx.doi.org/10.1039/C6SM01424K>.
- [77] M. Yang, A. Wysocki, and M. Ripoll, *Soft Matter* **10**, 6208 (2014), URL <http://dx.doi.org/10.1039/C4SM00621F>.
- [78] J. Hu, A. Wysocki, R. G. Winkler, and G. Gompper, *Sci. Rep.* **5**, 9586 (2015), URL <http://dx.doi.org/10.1038/srep09586>.
- [79] M. P. Allen and D. J. Tildesley, *Computer Simulation of Liquids* (Clarendon Press, Oxford, 1987).
- [80] C.-C. Huang, G. Gompper, and R. G. Winkler, *Phys. Rev. E* **86**, 056711 (2012).
- [81] K. Mussawisade, M. Ripoll, R. G. Winkler, and G. Gompper, *J. Chem. Phys.* **123**, 144905 (2005).
- [82] C.-C. Huang, A. Chatterji, G. Sutmann, G. Gompper, and R. G. Winkler, *J. Comp. Phys.* **229**, 168 (2010).
- [83] C.-C. Huang, A. Varghese, G. Gompper, and R. G. Winkler, *Phys. Rev. E* **91**, 013310 (2015), URL <http://link.aps.org/doi/10.1103/PhysRevE.91.013310>.
- [84] T. Ihle and D. M. Kroll, *Phys. Rev. E* **67**, 066706 (2003).
- [85] N. Kikuchi, C. M. Pooley, J. F. Ryder, and J. M. Yeomans, *J. Chem. Phys.* **119**, 6388 (2003).
- [86] C. M. Pooley and J. M. Yeomans, *J. Phys. Chem. B* **109**,

- 6505 (2005).
- [87] H. Noguchi and G. Gompper, Phys. Rev. E **78**, 016706 (2008).
- [88] R. G. Winkler and C.-C. Huang, J. Chem. Phys. **130**, 074907 (2009).
- [89] E. Westphal, S. P. Singh, C.-C. Huang, G. Gompper, and R. G. Winkler, Comput. Phys. Comm. **185**, 495 (2014).
- [90] M. Daoud and J. Cotton, Journal de Physique **43**, 531 (1982).
- [91] T. Birshtein, E. Zhulina, and O. Borisov, Polymer **27**, 1078 (1986).
- [92] S. P. Singh, C.-C. Huang, E. Westphal, G. Gompper, and R. G. Winkler, J. Chem. Phys. **141**, 084901 (2014), URL <http://scitation.aip.org/content/aip/journal/jcp/141/8/10.1063/1.4893766>.